Transform Image Coding

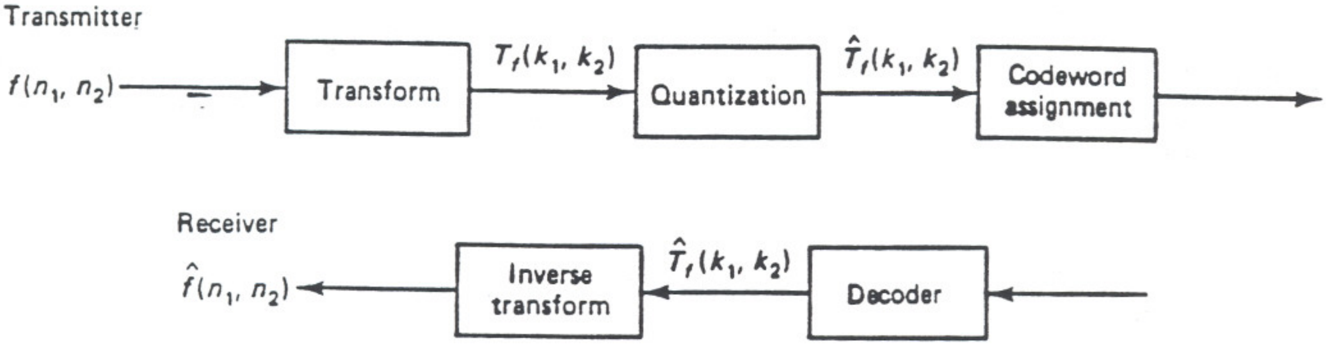

What is exploited: Most of the image energy is concentrated in a small number of coefficients for some transforms

- the more energy compaction, the better

Some considerations:

- energy compaction in a small number of coefficients
- computational aspect: important (subimage by sub-image coding — 8×8 - 16×16)
- transform should be invertible
- Correlation Reduction

Examples of Transforms

1. Karhunen-Loeve Transform

$$F_k(k_1, k_2) = \sum_{n=0}^{N_1-1} \sum_{n_2=0}^{N_2-1} f(n_1, n_2) \cdot A(n_1, n_2;\ k_1, k_2)$$

$$\lambda(k_1, k_2) \cdot A(n_1, n_2;\ k_1, k_2) =$$

$$\sum_{k_1=0}^{N_1-1} \sum_{k_2=0}^{N_2-1} K_f(n_1, n_2;\ l_1, l_2) \cdot A(l_1, l_2;\ k_1, k_2)$$

Covariance $K_f(n_1, n_2;\ l_1, l_2) =$

$$E\ [(x(n_1, n_2) - \overline{x}(n_1, n_2)) \cdot (x(l_1, l_2) - \overline{x}(l_1, l_2))]$$

Comments:

- optimal in the sense that the coefficients are completely uncorrelated
- finding $K_f(n_1, n_2;\ l_1, l_2)$ is hard
- no simple computational algorithm
- seldom used in practice
- On average, first M coefficients have more energy than any other transform
- KL is best among all linear transforms from: (a) compaction (b) decorrelation.

Fig. 5.3.7 Images used for coding and statistics. (a) "Karen" has much more stationary statistics than (b) "Stripes."

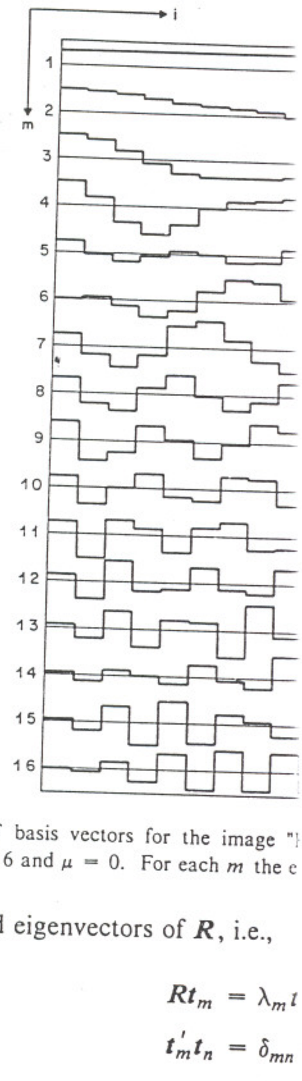

Fig. 5.3.8 KLT basis vectors for the image "I
N=16 and μ = 0. For each m the e

orthonormalized eigenvectors of $\boldsymbol{R}$, i.e.,

$$\boldsymbol{R t}_m = \lambda_m t$$

$$\boldsymbol{t}'_m \boldsymbol{t}_n = \delta_{mn}$$

where the eigenvalues $\{\lambda_m\}$ are nonnegati

For example, Fig. 5.3.8 shows KL "Karen" in Fig. 5.3.7a using one-dimensi and $\mu = 0$. The eigenvectors are arr eigenvalue. Note that, for the most part, according to increasing frequency, i.e., basis vector. Fig. 5.3.9 shows similar c correlation model defined in Chapter

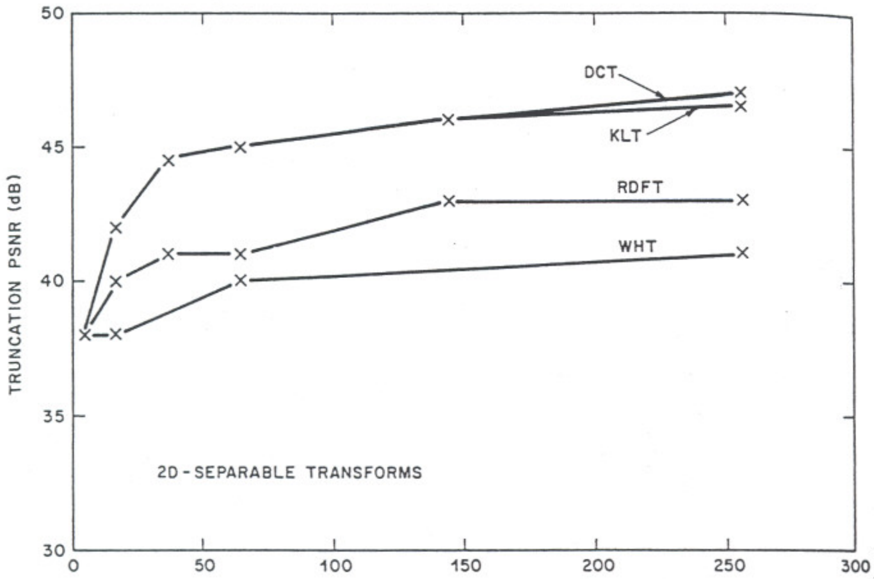

Fig. 5.3.22 Truncation PSNR versus block size for separable transforms with the image "Karen" when 60 percent of the coefficients are kept (p=0.6).

size, the higher the energy compaction achieved by the transform. Also two-dimensional blocks achieve more compaction than one-dimensional blocks. Experience has shown that over a wide range of pictures there is not much improvement in average energy compaction for two dimensional block sizes above 8×8 pels. However, individual pictures with higher nonstationary statistics can always be found for which this rule of thumb is violated (for example, compare the KLT curves of Fig. 5.3.17 and Fig.5.3.19). Also, considerable correlation may remain between blocks, even though the correlation between pels within a block is largely removed.[5.3.21] We shall return to this point in a later section.

5.3.1f Miscellaneous Transforms

Several other transforms have been studied. For example, the Haar Transform[5.3.8] can be computed from an orthogonal (but not orthonormal) matrix T that contains only +1's, −1's and zeros as shown in Fig. 5.3.23. This enables rather simple and speedy calculation, but at the expense of energy compaction performance.

Fig. 5.3.23 Haar transform matri
multiplications.

The Slant Transform[5.3.9]
vector t_1, a basis vector t_2 give

$$t_2 = \alpha(N-1, N-$$

where α is a normalization c
approximate the local behavior
compaction. However, the t_2
overall performance in most c
been developed for the Slant Tr
The Sine Transform[5.3.10]

$$t_{mi} = \sqrt{}$$

$$m,i = 1 \ldots$$

Its main utility arises when ima
sum of two uncorrelated images
statistics with a KLT that is app
The Singular Value Decor
the separable inverse transform

where U and V are unitary L t

constructed from a two-
the L-pel rows end-to-end.
ot only high adjacent pel
ls with separation L. Thus
y large not only at low
L, etc. Fig. 5.3.19 shows
e transform coded in this
ing the largest MSV are
an those of Fig. 5.3.17 by

els the most often used
using two L-dimensional
Recall that with separable
d transform the rows and

(5.3.56)

ansform coefficients. For
when the separable DCT
lata from "Stripes". Note
encies compared with the
ertical correlation in this

the results of separable
icture "Karen" when only
LT was derived from the
of pels. We see that the
separable KLT. This is
not adapt very well to
all block size of $1 \times L$ pels.
e DCT is only a few dB
9. It is this characteristic
sform of choice in many

NR results for $p = 60\%$.
proves as the block size
ely small for block sizes

important parameters
nts although the picture
lly, the larger the block

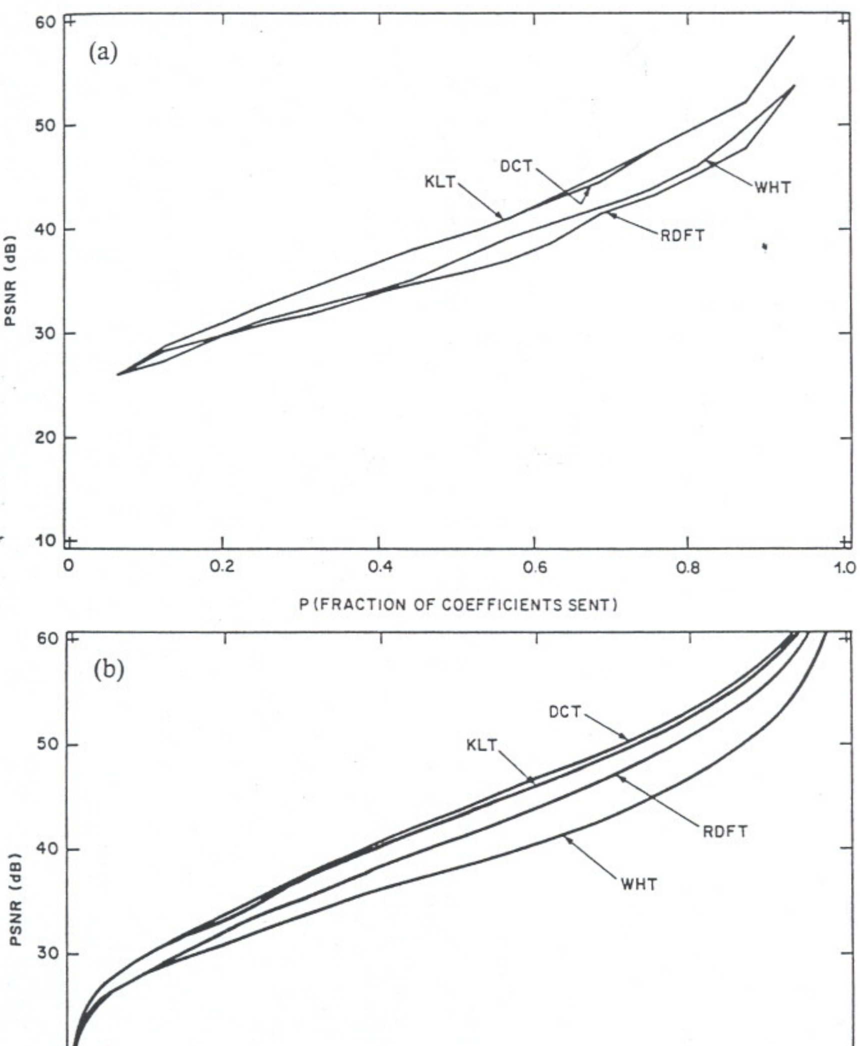

Fig. 5.3.21 Comparison of truncation errors using separable, two-dimensional blocks with the image "Karen". The coefficients having the largest MSV are transmitted. (a) 4×4 blocks, $N=16$. (b) 16×16 blocks, $N=256$.

Discrete Cosine Transform

$$f(n_1,n_2) \longrightarrow f'(n_1,n_2) = \frac{f(n_1,n_2)+f(n_1,-n_2)+f(-n_1,n_2)+f(-n_1,-n_2)}{4}$$

$$\downarrow$$

$$\boxed{\text{DFT}}$$

$$\downarrow$$

$$F_c(k_1,k_2)$$

Comments:

- good energy compaction (better than DFT)

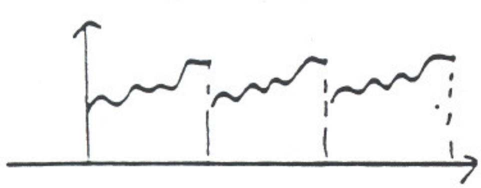

sharp discontinuity

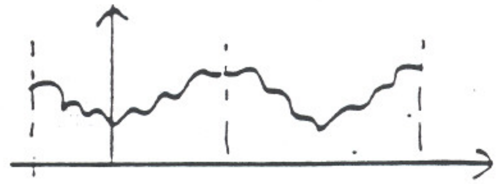

no sharp discontinuity

- fast algorithms
- all real coefficients
- most often used in practice (good quality image at bit rate less than 1 bit/pixel)
- other transforms: Hadamard, Haar, Slant, Sine, ...

The sequence $Y(k)$ is related to $y(n)$ through the $2N$-point inverse DFT relation given by

$$y(n) = \frac{1}{2N} \sum_{k=0}^{2N-1} Y(k) W_{2N}^{-kn}, \quad 0 \le n \le 2N - 1. \tag{3.28}$$

From (3.20), $x(n)$ can be recovered from $y(n)$ by

$$x(n) = \begin{cases} y(n), & 0 \le n \le N - 1 \\ 0, & \text{otherwise.} \end{cases} \tag{3.29}$$

From (3.27), (3.28), and (3.29), and after some algebra,

$$x(n) = \begin{cases} \dfrac{1}{N}\left[\dfrac{C_x(0)}{2} + \displaystyle\sum_{k=1}^{N-1} C_x(k) \cos \frac{\pi}{2N} k(2n + 1)\right], & 0 \le n \le N - 1 \\ 0, & \text{otherwise.} \end{cases} \tag{3.30}$$

Equation (3.30) can also be expressed as

$$x(n) = \begin{cases} \dfrac{1}{N} \displaystyle\sum_{k=0}^{N-1} w(k) C_x(k) \cos \frac{\pi}{2N} k(2n + 1), & 0 \le n \le N - 1 \\ 0, & \text{otherwise.} \end{cases} \tag{3.31a}$$

where

$$w(k) = \begin{cases} \dfrac{1}{2}, & k = 0 \\ 1, & 1 \le k \le N - 1. \end{cases} \tag{3.31b}$$

Equation (3.31) is the inverse DCT relation. From (3.25) and (3.31),

Discrete Cosine Transform Pair

$$C_x(k) = \begin{cases} \displaystyle\sum_{n=0}^{N-1} 2x(n) \cos \frac{\pi}{2N} k(2n + 1), & 0 \le k \le N - 1 \\ 0, & \text{otherwise.} \end{cases} \tag{3.32a}$$

$$x(n) = \begin{cases} \dfrac{1}{N} \displaystyle\sum_{k=0}^{N-1} w(k) C_x(k) \cos \frac{\pi}{2N} k(2n + 1), & 0 \le n \le N - 1 \\ 0, & \text{otherwise.} \end{cases} \tag{3.32b}$$

From the derivation of the DCT pair, the DCT and inverse DCT can be computed by

Computation of Discrete Cosine Transform

Step 1. $y(n) = x(n) + x(2N - 1 - n)$

Step 2. $Y(k) = \text{DFT}\,[y(n)]$ ($2N$-point DFT computation)

Step 3. $C_x(k) = \begin{cases} W_{2N}^{k/2} Y(k), & 0 \le k \le N - 1 \\ 0, & \text{otherwise} \end{cases}$

Computation of Inverse Discrete Cosine Transform

Step 1.
$$Y(k) = \begin{cases} W_{2N}^{-k/2} C_x(k), & 0 \le k \le N-1 \\ 0, & k = N \\ -W_{2N}^{-k/2} C_x(2N-k), & N+1 \le k \le 2N-1 \end{cases}$$

Step 2. $y(n) = \text{IDFT}\,[Y(k)]$ (2N-point inverse DFT computation)

Step 3.
$$x(n) = \begin{cases} y(n), & 0 \le n \le N-1 \\ 0, & \text{otherwise} \end{cases}$$

In computing the DCT and inverse DCT, Steps 1 and 3 are computationally quite simple. Most of the computations are in Step 2, where a 2N-point DFT is computed for the DCT and a 2N-point inverse DFT is computed for the inverse DCT. The DFT and inverse DFT can be computed by using fast Fourier transform (FFT) algorithms. In addition, because $y(n)$ has symmetry, the 2N-point DFT and inverse DFT can be computed (see Problem 3.20) by computing the N-point DFT and the N-point inverse DFT of an N-point sequence. Therefore, the computation involved in using the DCT is essentially the same as that involved in using the DFT.

In the derivation of the DCT pair, we have used an intermediate sequence $y(n)$ that has symmetry and whose length is even. The DCT we derived is thus called an even symmetrical DCT. It is also possible to derive the odd symmetrical DCT pair in the same manner. In the odd symmetrical DCT, the intermediate sequence $y(n)$ used has symmetry, but its length is odd. For the sequence $x(n)$ shown in Figure 3.9(a), the sequence $y(n)$ used is shown in Figure 3.9(b). The length of $y(n)$ is $2N - 1$, and $\tilde{y}(n)$, obtained by repeating $y(n)$ every $2N - 1$ points, has no artificial discontinuities. The detailed derivation of the odd symmetrical DCT is considered in Problem 3.22. The even symmetrical DCT is more commonly used, since the odd symmetrical DCT involves computing an odd-length DFT, which is not very convenient when one is using FFT algorithms.

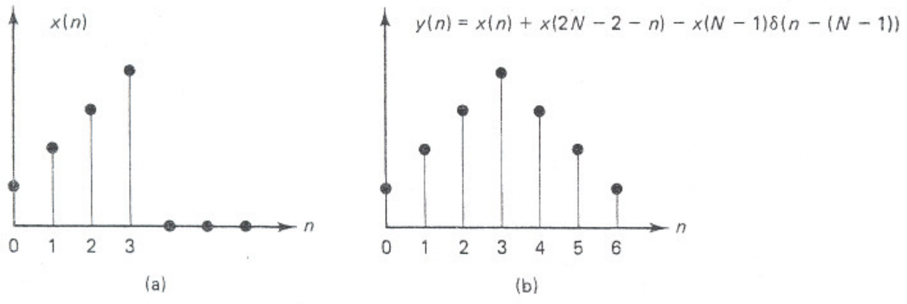

Figure 3.9 Example of (a) $x(n)$ and (b) $y(n) = x(n) + x(2N - 2 - n) - x(N - 1)\delta(n - (N - 1))$. The sequence $y(n)$ is used in the intermediate step in defining the odd symmetrical discrete cosine transform of $x(n)$.

DCT

- Signal independent

- ρ ---> 1 : KLT ---> DCT

  for first order
  Markov Image model

- Type II DCT:

$$S(K_1, K_2) = \sqrt{\frac{4}{N^2}} C(K_1) C(K_2)$$

$$\sum_{n_1 = o}^{N-1} \sum_{n_2 = o}^{N-1} s(n_1, n_2) \cos\left(\frac{\pi 2(n_1 + 1) K_1}{2N}\right)$$

$$\cos\left(\frac{\pi 2(n_2 + 1) K_2}{2N}\right)$$

$$C(K) = \begin{cases} \frac{1}{\sqrt{2}} & K = o \\ 1 & \text{otherwise} \end{cases}$$

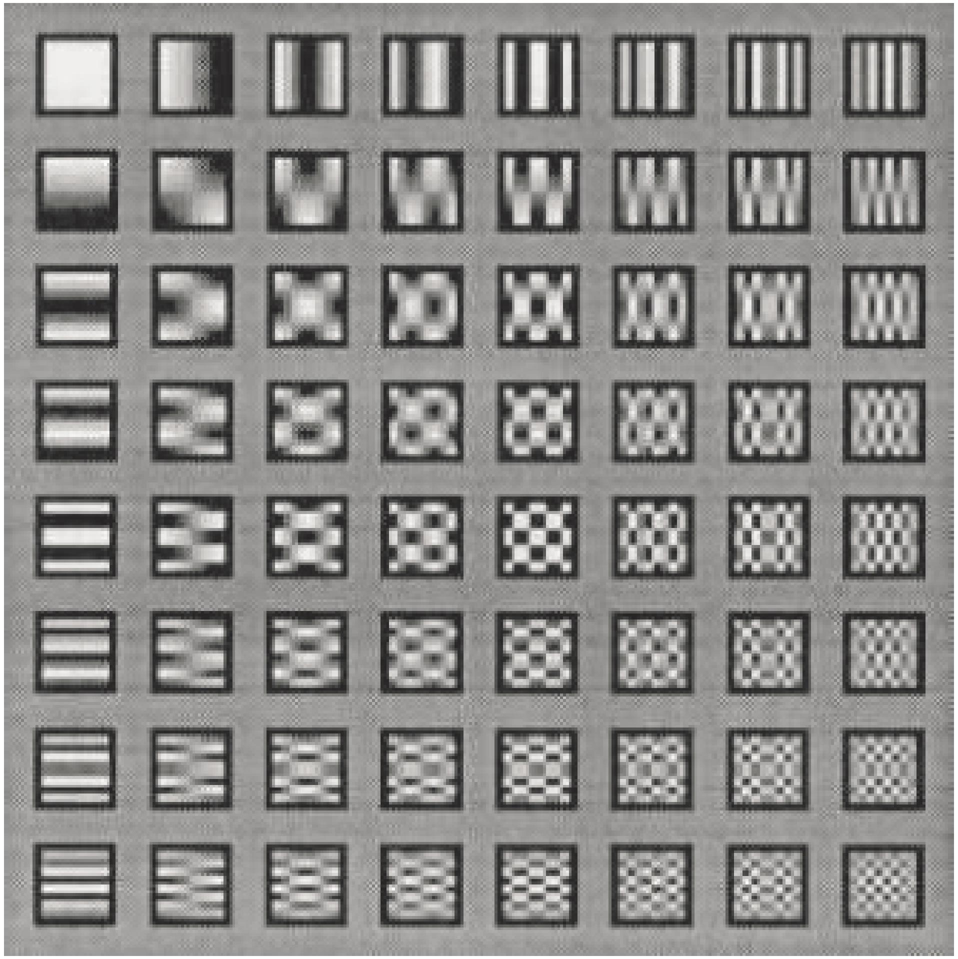

Discarding Transform Coefficients (cont.)

Threshold coding: Coefficients with values above a given threshold are coded

- location as well as amplitude has to be coded
- run-length coding is useful (many zeroes)

15	0	0	0	0	0	0	0	0	0	0	[illegible]	[illegible]	[illegible]	[illegible]	[illegible]	[illegible]
14	0	0	0	0	0	0	0	0	0	0	0	0	0	0	0	0
13	0	0	0	0	0	0	0	0	0	0	0	0	0	0	0	0
12	0	0	0	0	0	0	0	0	0	0	0	0	0	0	0	0
11	0	0	0	0	0	0	0	0	0	0	0	0	0	0	0	0
10	1	0	0	0	0	0	0	0	0	0	0	0	0	0	0	0
9	1	1	0	0	0	0	0	0	0	0	0	0	0	0	0	0
8	2	1	1	0	0	0	0	0	0	0	0	0	0	0	0	0
7	2	1	1	1	0	0	0	0	0	0	0	0	0	0	0	0
6	2	1	1	1	1	0	0	0	0	0	0	0	0	0	0	0
5	3	2	1	1	1	1	0	0	0	0	0	0	0	0	0	0
4	3	2	2	2	1	1	1	0	0	0	0	0	0	0	0	0
3	3	3	2	2	2	1	1	1	0	0	0	0	0	0	0	0
2	4	3	2	2	2	1	1	1	1	0	0	0	0	0	0	0
1	5	4	3	3	2	2	1	1	1	1	0	0	0	0	0	0
0	7	5	4	3	3	3	2	2	2	2	1	0	0	0	0	0
	0	1	2	3	4	5	6	7	8	9	10	11	12	13	14	15 → k_1

Figure 10.44 Example of bit allocation map at $\frac{1}{2}$ bit/pixel for zonal discrete cosine transform image coding. Block size = 16 × 16 pixels.

Discarding Transform Coefficients

Zonal coding: Eliminate coefficients in a fixed zone

(Ex)

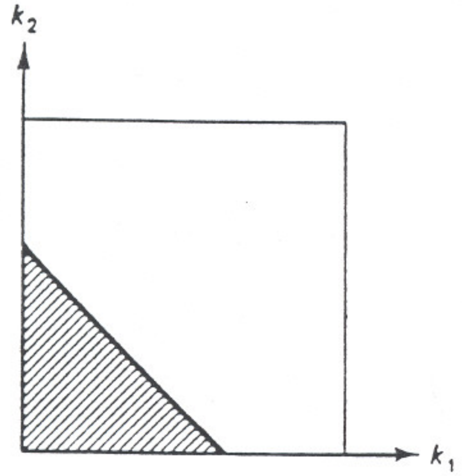

(a)

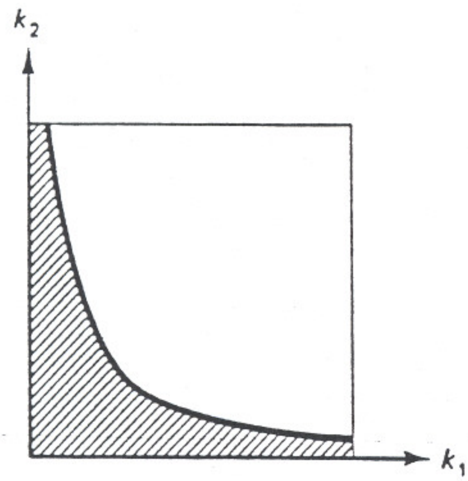

(b)

Bits for coefficient i with variance σ_i^2

$$b_i = \frac{B}{M} + \frac{1}{2}\log_2 \sigma_i^2 - \frac{1}{2M}\sum_{i=1}^{M} \log_2 \sigma_i^2$$

M = # of coefficients to be coded

B = Total # of bits

Scalar Quantization of a Vector Source

- Assume N scalars: $f_i \qquad 1 \leq i \leq N$
- Each f_i is quantized to L_i reconstruction levels.
- Total of B bits to code N scalars.
- Optimum bit allocation strategy depends on (a) error criterion and (b) pdf of each random variable.
- Assume we minimize MSE : $\Sigma_{i=1}^{N} E[(f\prime_i - f_i)^2]$ with respect to B_i the number of bits for the ith scalar for $1 \leq i \leq N$.
- Assume pdf of all f_i is the same except they have different variances.
- Use Lloyd Max quantizer.
- Under these conditions we have:

$$B_i = \frac{B}{N} + \frac{1}{2} log \frac{\sigma_i^2}{[\Pi_{j=1}^{N} \sigma_j^2]^{1/N}}$$

- σ_i^2 is the variance of f_i

$$L_i = \frac{\sigma_i}{[\Pi_{j=1}^{N} \sigma_i]^{1/N}} 2^{B/N}$$

- L_i is the number of reconstruction levels for source i

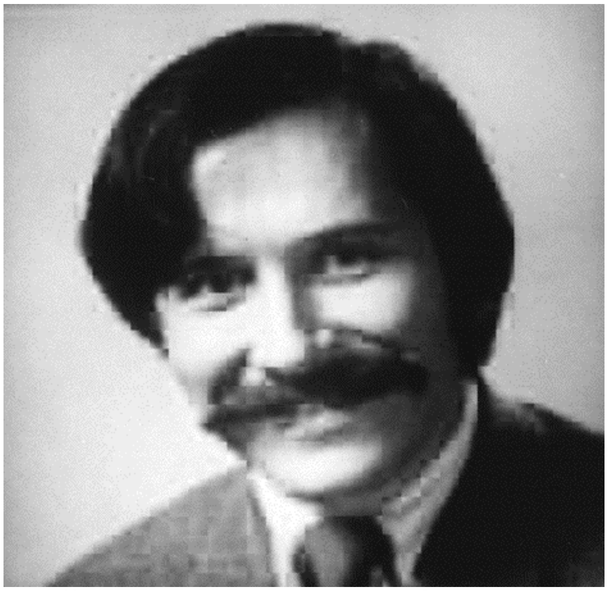

Figure 10.47 DCT-coded image with visible blocking effect.

and (b) show the results of DCT image coding at 1 bit/pixel and $\frac{1}{2}$ bit/pixel, respectively. The original image is the 512 × 512-pixel image shown in Figure 10.45(a). In both examples, the subimage size used is 16 × 16 pixels, and adaptive zonal coding with the zone shape shown in Figure 10.43(b) and the zone size adapted to the local image characteristics has been used.

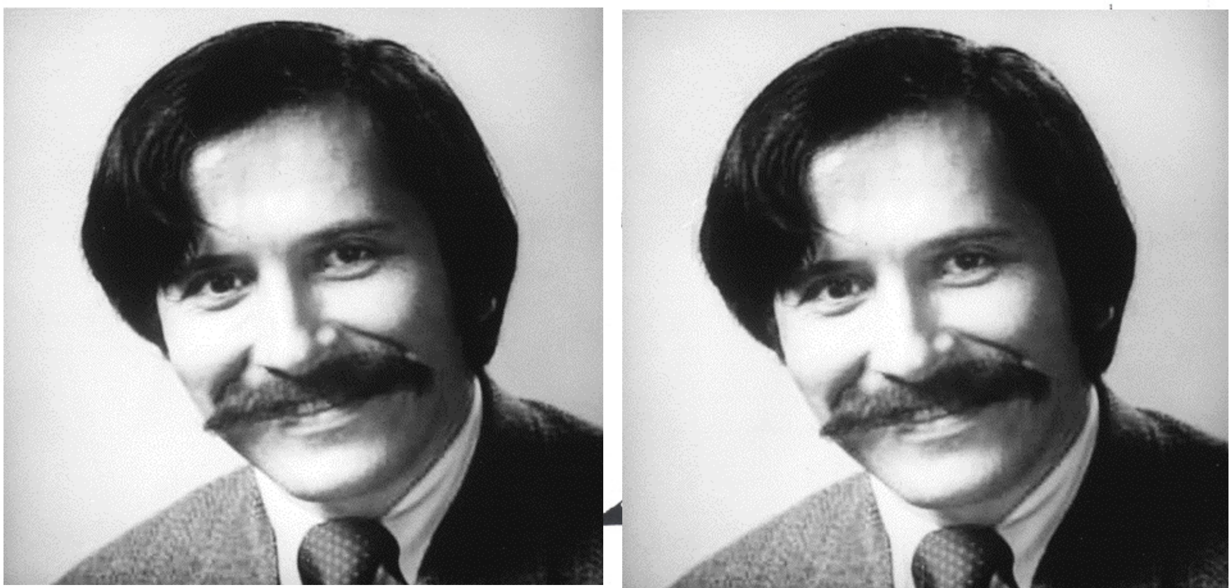

Figure 10.48 Example of DCT image coding. (a) DCT-coded image at 1 bit/pixel. NMSE = 0.8%, SNR = 20.7 dB. (b) DCT-coded image at 1/2 bit/pixel. NMSE = 0.9%, SNR = 20.2 dB.

280

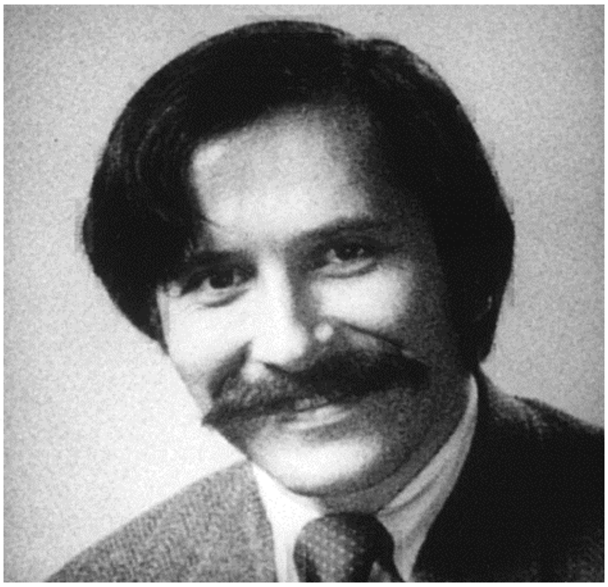

Figure 10.46 Illustration of graininess increase due to quantization of DCT coefficients. A 2-bit/pixel uniform quantizer was used to quantize each DCT coefficient retained to reconstruct the image in Figure 10.45(b).

and are selected from a zone of triangular shape shown in Figure 10.43(a). From Figure 10.45, it is clear that the reconstructed image appears more blurry as we retain a smaller number of coefficients. It is also clear that an image reconstructed from only a small fraction of the transform coefficients looks quite good, illustrating the energy compaction property.

Another type of degradation results from quantization of the retained transform coefficients. The degradation in this case typically appears as graininess in the image. Figure 10.46 shows the result of coarse quantization of transform coefficients. This example is obtained by using a 2-bit uniform quantizer for each retained coefficient to reconstruct the image in Figure 10.45(b).

A third type of degradation arises from subimage-by-subimage coding. Since each subimage is coded independently, the pixels at the subimage boundaries may have artificial intensity discontinuities. This is known as the *blocking effect*, and is more pronounced as the bit rate decreases. An image with a visible blocking effect is shown in Figure 10.47. A DCT with zonal coding, a subimage of 16 × 16 pixels, and a bit rate of 0.15 bit/pixel were used to generate the image in Figure 10.47.

Examples. To design a transform coder at a given bit rate, different types of image degradation due to quantization have to be carefully balanced by a proper choice of various design parameters. As was discussed, these parameters include the transform used, subimage size, selection of which coefficients will be retained, bit allocation, and selection of quantization levels. If one type of degradation dominates other types of degradation, the performance of the coder can usually be improved by decreasing the dominant degradation at the expense of some increase in other types of degradation.

Figure 10.48 shows examples of transform image coding. Figure 10.48(a)

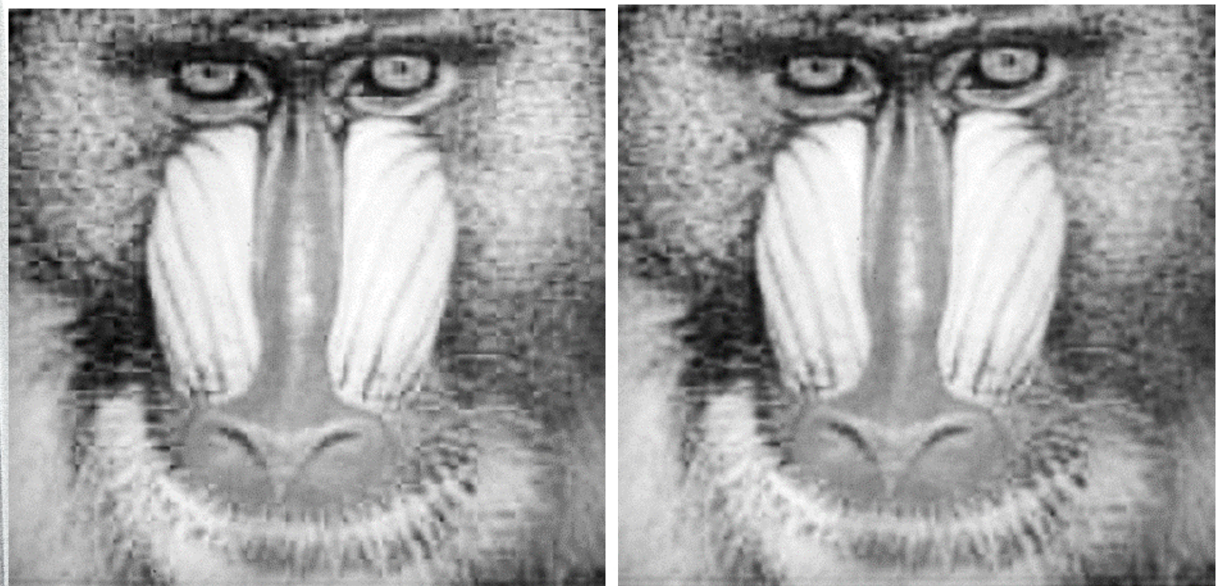

Figure 10.50 Example of blocking effect reduction using a filtering method. (a) Image of 512 $\times$ 512 pixels with visible blocking effect. The image is coded by a zonal DCT coder at 0.2 bit/pixel. (b) Image in (a) filtered to reduce the blocking effect. The filter used is a 3 $\times$ 3-point $h(n_1, n_2)$ with $h(0, 0) = \frac{1}{5}$ and $h(n_1, n_2) = \frac{1}{10}$ at the remaining eight points.

selection of the zone shape and size in zonal coding are simpler than those with a 2-D transform coder. Hybrid coding of a single image frame has not been used extensively in practice, perhaps because the method does not reduce the correlation in the data as much as a 2-D transform coder and the complexity in a 2-D transform coder implementation is not much higher than a hybrid coder. As will be discussed in Section 10.6, however, hybrid coding is useful in interframe image coding.

10.4.5 Adaptive Coding and Vector Quantization

Transform coding techniques can be made adaptive to the local characteristics within each subimage. In zonal coding, for example, the shape and size of the

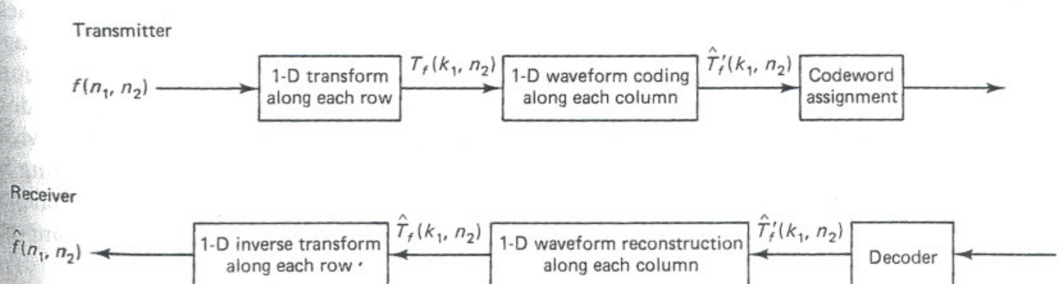

Figure 10.51 Hybrid transform/waveform coder.

Iterative Procedures for Reduction of Blocking Effects in Transform Image Coding

Ruth Rosenholtz and Avideh Zakhor

Abstract—**We propose a new iterative block reduction technique based on the theory of projection onto convex sets. The basic idea behind this technique is to impose a number of constraints on the coded image in such a way as to restore it to its original artifact-free form. One such constraint can be derived by exploiting the fact that the transform-coded image suffering from blocking effects contains high-frequency vertical and horizontal artifacts corresponding to vertical and horizontal discontinuities across boundaries of neighboring blocks. Since these components are missing in the original uncoded image, or at least can be guaranteed to be missing from the original image prior to coding, one step of our iterative procedure consists of projecting the coded image onto the set of signals that are bandlimited in the horizontal or vertical directions. Another constraint we have chosen in the restoration process has to do with the quantization intervals of the transform coefficients. Specifically, the decision levels associated with transform coefficient quantizers can be used as lower and upper bounds on transform coefficients, which in turn define boundaries of the convex set for projection. Thus, in projecting the "out-of-bound" transform coefficient onto this convex set, we will choose the upper (lower) bound of the quantization interval if its value is greater (less) than the upper (lower) bound. We present a few examples of our proposed approach.**

Manuscript received June 10, 1991; revised February 3, 1992. This work has been supported by IBM, Eastman Kodak Company, TRW, and the National Science Foundation contract MIP-9057466. This paper was recommended by Associate Editor Dimintris Anastassiou.

The author is with the Department of Electrical Engineering and Computer Sciences, University of California, Berkeley, CA 94720.

IEEE Log Number 9107519.

I. Introduction

Transform coding is one of the most widely used image compression techniques. It is based on dividing an image into small blocks, taking the transform of each block and discarding high-frequency coefficients and quantizing low-frequency coefficients. Among various transforms, the discrete cosine transform (DCT) is one of the most popular because its performance for certain class of images is close to that of the Karhunen–Loeve transform (KLT), which is known to be optimal in the mean squared error sense.

Although DCT is used in most of today's standards such as JPEG and MPEG, its main drawback is what is usually referred to as the "blocking effect." Dividing the image into blocks prior to coding causes blocking effects—discontinuities between adjacent blocks—particularly at low bit rates. In this paper, we present an iterative technique for the reduction of blocking effects in coded images.

II. Iterative Restoration Method

The block diagram of our proposed iterative approach is shown in Fig. 1. The basic idea behind our technique is to impose a number

1051-8215/92$03.00

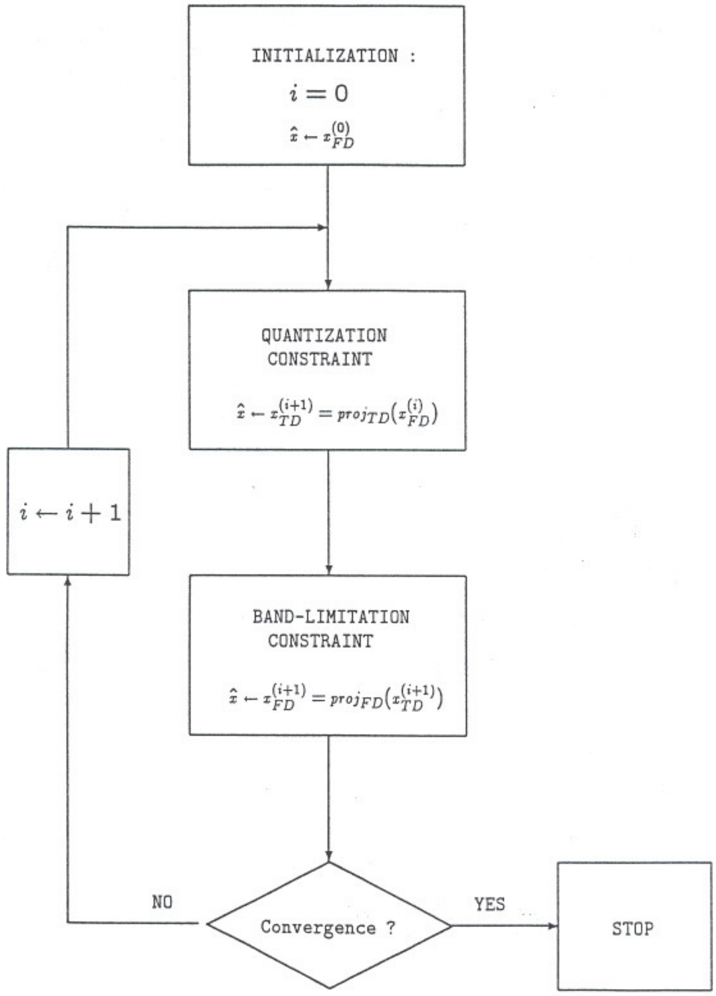

Fig. 1. Block diagram of the iterative algorithm.

of constraints on the coded image in such a way as to restore it to its original artifact-free-form. We derive one such constraint from the fact that the coded image with $N \times N$ blocks has high-frequency horizontal and vertical artifacts corresponding to the discontinuities at the edges of the $N \times N$ blocks. Therefore, one step of our procedure consists of bandlimiting the image in the horizontal and vertical directions. We refer to this constraint as the filtering constraint.

We derive the second constraint from the quantizer and thus refer to it as the quantization constraint. Because the quantization intervals for each DCT coefficient is assumed to be known in decoding a DCT encoded image, the quantization constraint ensures that in restoring images with blocking effects, DCT coefficients of $N \times N$ blocks remain in their original quantization interval.

If S_1 denotes the set of bandlimited images, and S_2 denotes the set of images whose $N \times N$ DCT coefficients lie in specific quantization intervals, our goal can be stated as that of finding an image in the intersection of S_1 and S_2. One way to achieve this is to start with an arbitrary element in either of the two sets and iteratively map it back and forth to the other set, until the process converges to an element in the intersection of the two sets. Under these conditions convergence can be guaranteed by the theory of projection onto convex sets (POCS) if sets S_1 and S_2 are convex, and if the mapping from each set to the other is a projection [6]. By definition, the projection of an element x in set A onto set B is equivalent to finding the closest element, according to some metric, in B to x.

To apply the above idea to our problem, we first notice that two sets S_1 and S_2 are both convex. We also choose the mean squared error as our metric of closeness. This implies that a projection from S_2 to S_1 can be accomplished by any bandlimitation algorithm such as ideal low-pass filtering. It also implies that projection from S_1 to S_2 can be accomplished by moving $N \times N$ DCT coefficients that are outside their designated quantization interval to the closest boundary of their respective quantization intervals. For instance, if a particular $N \times N$ DCT coefficient, which is supposed to be in the range $[a, b]$, takes on a value greater than b, it is projected to b. Alternatively, if it takes on a value smaller than a it is projected onto a.

Having explained the constraints, convex sets, and projections, we now summarize our proposed iterative procedure shown in Fig. 1. In the first part of each iteration, we low pass filter, or bandlimit, the image that has high-frequency horizontal and vertical components corresponding to the discontinuities between $N \times N$ blocks. In the second part of each iteration we apply the quantization constraint as follows. First we divide the image into $N \times N$ blocks and take the DCT of each. Then we project any coefficient outside its quantization range onto its appropriate value. Under these conditions, the POCS theory guarantees that iterative projection between the sets S_1 and S_2 results in convergence to an element in the intersection of the two sets.

III. Experimental Results

Fig. 2(a) shows the original, unquantized 512×512 Lena, and (b), (c), and (d) show its JPEG encoded version to 0.43, and 0.24,

(a)

(b)

(c)

(d)

Fig. 2(a) Original 512 × 512 image, Lena. 2(b) Lena quantized to 0.43 bpp. 2(c) Lena quantized to 0.24 bpp. 2(d) Lena quantized to 0.15 bpp.

and 0.15 bpp, respectively. The quantization tables for Figs. 2(b), (c), and (d) are included in the Appendix.

Strictly speaking, the band-limitation portion of our algorithm corresponds to a true projection if the image under consideration is convolved with an ideal low-pass filter. Since an ideal low-pass filter cannot be implemented in practice, we have chosen to approximate it with a 3 × 3 finite impulse response (FIR) filter of the form

$$\begin{aligned} &h(0,0) = 0.2042, \\ &h(0,1) = h(0,-1) = h(1,0) = h(-1,0) = 0.1239 \quad (1) \\ &h(0,2) = h(0,-2) = h(2,0) = h(2,0) = 0.0751. \end{aligned}$$

We now show examples of our iterative algorithm. Fig. 3(a) shows five iterations of our algorithm applied to the 0.43-bpp quantized image of Fig. 2(b). The FIR filter of (1) was used for the band-limitation step. As Fig. 2(b) shows, blocking artifact has been removed without introducing excessive blurring. For comparison purposes, the result of applying the low-pass filter in (1) to Fig. 2(b) for five times, without applying the quantization constraint, is also shown in Fig. 3(b). Although consecutive low-pass filtering removes most of the blocking effect, it blurs the image in a noticeable way. We have found that applying the low-pass filter of (1) once rather than five times, results in a less blurry image than in Fig. 3(b), but at the same time does not remove all the blocking effect.

Figs. 4(a) and (b) show application of our algorithm to the 0.24-bpp quantized image of Fig. 2(c) for 5 and 20 iterations, respectively. The FIR filter of (1) was used for the band-limitation step. As seen, the blocking artifact is better removed in Fig. 4(b) than in 4(a), while they are as sharp as each other. For comparison purposes, Fig. 4(c) and (d) show the result of applying the low-pass filter of (1) to Fig. 2(c), 5 and 20 times, respectively. Comparing Fig. 4(c) and 4(d) to Fig. 4(a) and (b), respectively, we find that the latter pair are more blurry than the former. Thus, applying the quantization constraint prevents the images from becoming excessively blurry.

Fig. 5(a) shows application of our algorithm to the 0.15-bpp quantized image of Fig. 2(d) for 20 iterations. The FIR filter of (1) was used for the band-limitation step. For comparison purposes, Fig. 5(b) shows the result of applying the low-pass filter of (1) to Fig. 2(d), 20 times. Comparing Fig. 5(b) to 5(a), we find that the latter is considerably more blurry than the former.

IV. Conclusions

The major conclusions to be drawn from this paper are as follows: 1) the proposed iterative algorithm using a 3 × 3 low-pass filtering of (1) results in images that are free of blocking artifacts and excessive blurring; 2) low-pass filtering by itself could remove blockiness but at the expense of increased blurriness.

It is conceivable to generate images similar to Figs. 5(a) and 4(b) without having to apply our algorithm for as many as 20 iterations. Our conjecture is that this could be achieved by increasing the region of support of the impulse response of the filter of (1). In practical hardware implementations however, 3 × 3 convolvers are more readily available than, say, 30 × 30 ones.

We have checked the convergence of our algorithm and found that it converges after 20 iterations or so. This is encouraging since there is no guarantee that the intersections of our particular convex sets is nonempty, and the theory of POCS only guarantees convergence in situations where the intersection is nonempty.

One way to increase the likelihood of convergence is to vary the confidence with which the ideal solution is in the chosen constraint set, by varying its size. For example, if we choose prototype constraint sets as in [10], using the statistics of the

(a)

(b)

Fig. 3(a) Result of applying the iterative algorithm to Fig. 2(b) for five iterations with the low-pass filter of (1) used for bandlimitation. (b) Result of low-pass filtering Fig. 2(b) five times using the filter in (1).

quantization noise, we can change the boundaries and the size of the constraint set in a controlled fashion and therefore increase the likelihood of a solution in the intersection of the constraint sets. Examples of such prototype constraint sets include bounded variation from the Weiner solution and pointwise adaptive smoothness. The latter constraint has the obvious advantage of being locally adaptive to changes in the characteristics of the image. Projection onto fuzzy sets is another way of increasing the size of our convex sets [9].

Appendix

The quantization table for Fig. 2(b) is

20	24	28	32	36	80	98	144
24	24	28	34	52	70	128	184
28	28	32	48	74	114	156	190
32	34	48	58	112	128	174	196
36	52	74	112	136	162	206	224
80	70	114	128	162	208	242	200
98	128	156	174	206	242	240	206
144	184	190	196	224	200	206	208

For Fig. 2(c) it is

50	60	70	70	90	120	255	255
60	60	70	96	130	255	255	255
70	70	80	120	200	255	255	255
70	96	120	145	255	255	255	255

(a)

(b)

(c)

(d)

Fig. 4(a) Result of applying the iterative algorithm to Fig. 2(c) for 5 iterations with the low-pass filter of (1) used for bandlimitation. (b) Result of applying the iterative algorithm to Fig. 2(c) for 20 iterations with the low-pass filter of (1) used for bandlimitation. (c) Result of low-pass filtering Fig. 2(c) five times using the filter in (1). (d) Result of low-pass filtering Fig. 2(c) 20 times using the filter in (1).

(a)

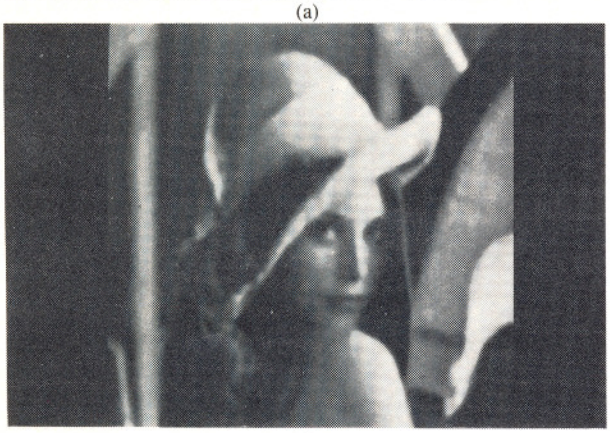

(b)

Fig. 5(a) Result of applying the iterative algorithm to Fig. 2(d) for 20 iterations with the low-pass filter of (1) used for bandlimitation. (b) Result of low pass filtering Fig. 2(d) 20 times using the filter in (1).

90	130	200	255	255	255	255	255
120	255	255	255	255	255	255	255
255	255	255	255	255	255	255	255
255	255	255	255	255	255	255	255

and for Fig. 2(d) it is:

110	130	150	192	255	255	255	255
130	150	192	255	255	255	255	255
150	192	255	255	255	255	255	255
192	255	255	255	255	255	255	255
255	255	255	255	255	255	255	255
255	255	255	255	255	255	255	255
255	255	255	255	255	255	255	255
255	255	255	255	255	255	255	255

The 255 entry in the above tables indicates that the coefficient was discarded.

References

[1] H. C. Reeve and J. S. Lim, "Reduction of blocking effects in image coding," *Optical Eng.*, vol. 23, no. 1, pp. 34–37, Jan./Feb. 1984.

[2] J. Biemond, R. L. Lagendijk, and R. M. Mersereau, "Iterative methods for image deblurring," *Proc. IEEE*, vol. 78, no. 5, pp. 856–883, May 1990.

[3] S. N. Efstratiadis and A. K. Katsaggelos, "Adaptive iterative image restoration with reduced computational load," *Optical Eng.*, vol. 29, no. 12, pp. 1458–1468, Dec. 1990.

[4] S. J. Reeves and R. M. Mersereau, "Optimal estimation of the regularization parameter and stabilizing functional for regularized image restoration," *Opt. Eng.*, vol. 29, no. 5, pp. 446–454, May 1990.

[5] B. J. Sullivan and A. K. Katsaggelos, "New termination rule for linear iterative image restoration algorithms," *Opt. Eng.*, vol. 29 no. 5, pp. 471–477, May 1990.

[6] D. C. Youla and H. Webb, "Image restoration by the method of convex projections: Part I—Theory," *IEEE Trans. Med. Imag.* vol. 1, no. 2, pp. 81–94, Oct. 1982.

[7] A. Zakhor and A. V. Oppenheim, "Reconstruction of two-dimensional signals from level crossings," *Proc. IEEE*, vol. 78, no. 1, pp. 31–55, Jan. 1990.

[8] A. Abo-Taleb and M. M. Fahmy, "Design of FIR two-dimensional digital filters by successive projections," *IEEE Trans. Circuits Syst.*, vol. CAS-31, no. 9, pp. 801–805, Sept. 1984.

[9] M. R. Civanlar and H. J. Trussell, "Digital image restoration using fuzzy sets," *IEEE Trans. Acoust. Speech, Signal Processing*, vol. 34, pp. 919–936, 1986.

[10] "Set-theoretic image restoration," *IEEE Trans. Signal Processing*," *vol.* 39, *no.* 10, *pp.* 2275-2285, *Oct.* 1991.

Fig. 6. Deblocking results for the decoded intra picture of the Container Ship sequence (QCIF, QP = 17).

(a)
Original

(b)
No filtering

(c)
POCS '92 [6]

(d)
POCS '93 [7]

(e)
VM 5.0 [10]

(f)
Proposed method